

Spatially self-similar spherically symmetric perfect-fluid models

Martin Goliath [†], Ulf S Nilsson [†] and Claes Uggla [‡]

[†] Department of Physics, Stockholm University, Box 6730,
S-113 85 Stockholm, Sweden

[‡] Department of Physics, Luleå University of Technology,
S-951 87 Luleå, Sweden

Abstract. Einstein's field equations for spatially self-similar spherically symmetric perfect-fluid models are investigated. The field equations are rewritten as a first-order system of autonomous differential equations. Dimensionless variables are chosen in such a way that the number of equations in the coupled system is reduced as far as possible and so that the reduced phase space becomes compact and regular. The system is subsequently analysed qualitatively with the theory of dynamical systems.

PACS numbers: 0420, 0420J, 0440N, 9530S, 9880H

1. Introduction

Spherically symmetric self-similar perfect fluid spacetimes have attracted considerable attention during the last couple of decades (see e.g., [1, 2] for references). This is not surprising since they lead to ordinary differential equations while still providing an arena for a number of interesting physical phenomena: shock waves [3, 4]; self-similar perturbations of the flat Friedmann-Lemaître-Robertson-Walker (FLRW) solution, which are of relevance for the growth of primordial black holes and evolution of voids (see, e.g., [1, 5, 6]); and violation of cosmic censorship [7], are some examples. These models also have broader implications. For example, they have turned out to be of essential importance when it comes to understanding spherically symmetric black hole formation [8, 9].

Self-similar spherically symmetric perfect-fluid models exhibit several preferred geometric structures. There are preferred directions associated with the 4-velocity of the fluid and the homothetic Killing vector (with self-similar spacetimes here we mean spacetimes with a homothetic Killing vector. For a discussion about self-similarity, see [10]). Another preferred structure is the area of the spherical symmetry surfaces. These three structures have led to three approaches, each using a specific coordinate gauge. The first is ‘the comoving perfect-fluid approach’ initiated by Cahill and Taub [3]. The second is ‘the homothetic approach’ used by Bogoyavlensky and co-workers [4, 11, 12]. The third is ‘the Schwarzschild approach’ used by, for example, Ori and Piran (see, e.g., [7]). Each gauge suggests more or less natural variables and each gauge has its individual physical interpretational advantages. Thus they are all complementary. However, it is possible to express many features gauge invariantly. This makes it possible to algebraically relate the variables one has used in the various approaches (this will be done in Appendix B). It is worth mentioning that apart from the above three approaches there are also some other approaches, useful for studying the spacetime structure ‘near’ singularities and for investigating global spacetime features, based on synchronous coordinate systems [4] and null coordinates [13].

We will use the homothetic approach as our starting point. The homothetic approach has the advantage that it reveals a considerable structural similarity between the field equations for the self-similar spherically symmetric models and the hypersurface homogeneous models (e.g. spatially homogeneous (SH) models). There is a considerable literature about how one can treat the field equations of the hypersurface homogeneous models. Thus the homothetic approach makes it possible to transfer ideas from the hypersurface homogeneous arena to the present situation. However, the homothetic approach, where one chooses a coordinate along the orbits of the homothetic Killing vector (see, e.g., [14, 15, 16]), has a disadvantage. In general, the symmetry surface changes causality. If one uses a homothetic diagonal gauge for the spherically symmetric case, then the spacetime must be covered with several coordinate patches; one for the region where the homothetic Killing vector is spacelike and one where it is timelike. Then one has to join the regions where the homothetic Killing vector is null.

This is the first paper in a series with the aim of obtaining a global picture of the space of solutions for self-similar spherically symmetric perfect-fluid models. Here we will consider the case where the homothetic Killing vector is spacelike; the so-called spatially self-similar (SSS) spherically symmetric models. These models are characterized by a four-dimensional homothetic symmetry group acting multiply transitively on three-dimensional spatial surfaces. In a subsequent paper [17] we will

deal with the timelike self-similar (TSS) spherically symmetric perfect-fluid models, i.e. the models where the homothetic Killing vector is timelike. Most of the physically interesting phenomena, e.g. shock waves, are actually associated with the TSS region, and consequently it is not surprising that most previous work has focused on this region. However, to obtain a global understanding one also needs to consider the spatial region. In a third paper we will address the specific problem of matching solutions between the two regions as well as focusing more on physical properties of the space of solutions. Therefore the mathematical nature of the present paper is justified as the results are needed in the subsequent studies. However, one physically interesting property pertaining to the SSS region, density perturbations of the flat FLRW solution, is treated in the present paper.

By using the homothetic approach and ideas from hypersurface homogeneous models we will reformulate Einstein's field equations so that the dynamics takes place in a reduced and compact phase space; one system for the spacelike case and one for the timelike case. Moreover, it will turn out that in our formulation, all equilibrium points (critical points, singular points, fixed points) are hyperbolic (here we also include the case of a line of equilibrium points where there is one zero eigenvalue corresponding to the line). This is in stark contrast to earlier treatments where noncompact variables have been used and where certain parts of phase space have been 'crushed'. To deal with these problems, one has made numerous variable changes and special treatments of various parts of phase space (see, e.g. [4]). This has resulted in an incomplete, or even misleading, picture of the global solution structure.

The line element for SSS spherically symmetric models, written in diagonal form where one of the coordinates is adapted to the homothetic symmetry, takes the form [4]

$$d\tilde{s}^2 = e^{2x} ds^2 = e^{2x} [-dt^2 + D_1^2(t) dx^2 + D_2^2(t) (d\theta^2 + \sin^2(\theta) d\varphi^2)]. \quad (1)$$

We will consider perfect fluid models. The energy momentum tensor, \tilde{T}_{ab} , is thus given by

$$\tilde{T}_{ab} = \tilde{\mu} u_a u_b + \tilde{p} (u_a u_b + \tilde{g}_{ab}), \quad (2)$$

where $\tilde{\mu}$ is the energy density, \tilde{p} is the pressure and u^a the 4-velocity of the fluid. We will assume

$$\tilde{p} = (\gamma - 1) \tilde{\mu}, \quad (3)$$

as an equation of state, where the parameter γ takes values in the interval $1 < \gamma < 2$ which include radiation ($\gamma = \frac{4}{3}$). Consequently, we have excluded dust ($\gamma = 1$) and stiff fluids ($\gamma = 2$). These models behave quite differently compared to those in the above interval, and thus need special treatment. The dust solutions are known explicitly (these models are just special cases of the general spherically symmetric dust solutions, which are all known explicitly, see e.g., [18]).

The outline of the paper is the following. In section 2 Einstein's field equations are rewritten in terms of a dimensionless set of variables in order to obtain a maximal reduction of the coupled system of ordinary differential equations. The variables are chosen so that they take values in a compact phase space. In section 3 the equations are subsequently analysed by means of methods from the theory of dynamical systems. In section 4 a numerical investigation is undertaken and global dynamical features are considered. We end with a discussion in section 5. Appendix A describes the properties of the fluid congruence, the condition for the spacetimes to belong to Petrov type 0

and also some expressions relevant for the mass function and density perturbations. Appendix B gives the relation between various coordinates and the relation between the present variables and other variables used in the literature.

2. The dynamical system

Following [19] we introduce

$$\begin{aligned} D_1 &= B_1^{-1} = e^{\beta^0 - 2\beta^+}, & D_2 &= B_2^{-1} = e^{\beta^0 + \beta^+}, \\ \theta &= 3\dot{\beta}^0, & \sigma_+ &= 3\dot{\beta}^+, \end{aligned} \quad (4)$$

where the dot denotes d/dt . The quantities θ and σ_+ describe the kinematical properties of the normal congruence of the symmetry surfaces in the (M, ds^2) spacetime that is conformally related to the physical spacetime $(M, d\tilde{s}^2)$ with the homothetic factor (see, e.g., [16]); θ is the expansion while σ_+ describes the shear. The orthonormal frame components, in (M, ds^2) , of the fluid velocity are conveniently parametrized by $(1, v, 0, 0)/\sqrt{1-v^2}$, where v is just the 3-velocity with respect to the symmetry surfaces. Einstein's field equations, $\tilde{G}_{ab} = \tilde{T}_{ab}$, and the conservation equations, $\tilde{T}^{ab}_{;b} = 0$, lead to a set of equations presented in [19]. However, for mathematical reasons we will now go over to another set of variables. The motivation lies in a simplification of the constraint while keeping the 'canonical quadratic' nature of the defining equation for μ_n (see the equations below). The new variables are given by

$$\begin{aligned} \bar{\theta} &= \frac{1}{\sqrt{3}}(2\theta - \sigma_+), & \bar{\sigma}_+ &= \frac{1}{\sqrt{3}}(-\theta + 2\sigma_+), \\ \theta &= \frac{1}{\sqrt{3}}(2\bar{\theta} + \bar{\sigma}_+), & \sigma_+ &= \frac{1}{\sqrt{3}}(\bar{\theta} + 2\bar{\sigma}_+). \end{aligned} \quad (5)$$

This leads to:

Evolution equations

$$\begin{aligned} \dot{\bar{\theta}} &= -\frac{1}{\sqrt{3}} \left[\bar{\theta}^2 + \bar{\sigma}_+^2 + \bar{\theta}\bar{\sigma}_+ - 3B_1^2 + \frac{3(\gamma-1)(1-v^2)}{1+(\gamma-1)v^2} \mu_n \right], \\ \dot{\bar{\sigma}}_+ &= -\frac{1}{\sqrt{3}} \left[\bar{\sigma}_+^2 + 2\bar{\theta}\bar{\sigma}_+ + \frac{3(2-\gamma) + (3\gamma-2)v^2}{2(1+(\gamma-1)v^2)} \mu_n \right], \\ \dot{B}_1 &= \frac{1}{\sqrt{3}} \bar{\sigma}_+ B_1, \\ \dot{B}_2 &= -\frac{1}{\sqrt{3}} (\bar{\theta} + \bar{\sigma}_+) B_2, \\ \dot{v} &= \frac{1-v^2}{\sqrt{3}\gamma(1-(\gamma-1)v^2)} \left\{ \gamma [2(\gamma-1)\bar{\theta} + \gamma\bar{\sigma}_+] v \right. \\ &\quad \left. + \sqrt{3} [(\gamma-1)(3\gamma-2)v^2 - (2-\gamma)] B_1 \right\}. \end{aligned} \quad (6)$$

Constraint equation

$$\gamma v \mu_n - \frac{2}{\sqrt{3}} [1 + (\gamma-1)v^2] \bar{\sigma}_+ B_1 = 0. \quad (7)$$

Defining equation for μ_n

$$\mu_n = \frac{1}{3} (\bar{\theta}^2 - \bar{\sigma}_+^2 - 3B_1^2 + 3B_2^2). \quad (8)$$

Auxiliary equation

$$\dot{\mu}_n = \frac{-\gamma\mu_n}{\sqrt{3}[1 + (\gamma - 1)v^2]} \left[2\bar{\theta} + (1 - v^2)\bar{\sigma}_+ + 2\sqrt{3}vB_1 \right]. \quad (9)$$

The quantity μ_n is the energy density of the fluid measured by an observer with the 4-velocity orthogonal to the symmetry surfaces in (M, ds^2) , see [16].

As the final step we will introduce a new set of variables where the scale invariance is used to decouple one equation. In spatially homogeneous cosmologies one often uses the expansion for this purpose. However, a very desirable property is to obtain a reduced phase space which is compact. Unfortunately, using, for example, θ or $\bar{\theta}$ does not achieve this in the present case. Instead we will use the quantity $\bar{\theta}^2 + 3B_2^2$ since this is a ‘dominant quantity’ (see equation (8)) and note that we assume a nonnegative energy density). We define a new variable Y ,

$$Y = \sqrt{\bar{\theta}^2 + 3B_2^2}, \quad B_2 = \sqrt{(Y^2 - \bar{\theta}^2)/3}. \quad (10)$$

Unfortunately, this will lead to a more mathematical treatment than if one uses a more ‘physical’ quantity instead of Y . However, there seems to be no such quantity which leads to a compact phase space. Instead one is forced to algebraically relate interesting physical objects, e.g. fluid kinematic quantities and mass functions to the variables used in this paper. These relations are given in Appendix A. We also introduce the Y -normalized bounded dimensionless variables

$$\bar{Q}_0 = \frac{\bar{\theta}}{Y}, \quad \bar{Q}_+ = \frac{\bar{\sigma}_+}{Y}, \quad \bar{C}_1 = \frac{\sqrt{3}B_1}{Y}. \quad (11)$$

Note that \bar{C}_1 is positive. The density μ_n is replaced by the density parameter Ω_Y , which is defined by

$$\Omega_Y = \frac{3\mu_n}{Y^2}. \quad (12)$$

An introduction of a dimensionless time variable $\bar{\tau}$

$$dt = \sqrt{3}Y^{-1}d\bar{\tau}, \quad (13)$$

leads to a decoupling of the Y -equation

$$Y' = F_Y Y, \quad F_Y = - \left[\bar{Q}_+ + \bar{Q}_0 \left(2\bar{Q}_+^2 + \frac{\gamma}{1 + (\gamma - 1)v^2} \Omega_Y \right) \right], \quad (14)$$

where a prime denotes $d/d\bar{\tau}$. The remaining coupled evolution equations can now be written in dimensionless form:

Evolution equations

$$\begin{aligned}
\bar{Q}'_0 &= -(1 - \bar{Q}_0^2) \left[\bar{Q}_+^2 - \bar{C}_1^2 + \frac{(\gamma - 1)(1 - v^2)}{1 + (\gamma - 1)v^2} \Omega_Y \right], \\
\bar{Q}'_+ &= -\bar{Q}_0 \bar{Q}_+ \left[2(1 - \bar{Q}_+^2) - \frac{\gamma \Omega_Y}{1 + (\gamma - 1)v^2} \right] \\
&\quad - \frac{1}{2} \frac{(2 - \gamma) + (3\gamma - 2)v^2}{1 + (\gamma - 1)v^2} \Omega_Y, \\
\bar{C}'_1 &= 2\bar{C}_1 \left[\bar{Q}_+ + \bar{Q}_0 \bar{Q}_+^2 + \frac{1}{2} \frac{\gamma}{1 + (\gamma - 1)v^2} \bar{Q}_0 \Omega_Y \right], \\
v' &= \frac{1 - v^2}{\gamma [1 - (\gamma - 1)v^2]} \left\{ \gamma [2(\gamma - 1)\bar{Q}_0 + \gamma \bar{Q}_+] v + \right. \\
&\quad \left. [(\gamma - 1)(3\gamma - 2)v^2 - (2 - \gamma)] \bar{C}_1 \right\}.
\end{aligned} \tag{15}$$

Constraint equation

$$G \equiv \gamma v \Omega_Y - 2(1 + (\gamma - 1)v^2) \bar{Q}_+ \bar{C}_1 = 0. \tag{16}$$

Defining equation for Ω_Y

$$\Omega_Y = 1 - \bar{Q}_+^2 - \bar{C}_1^2. \tag{17}$$

Auxiliary equation

$$\Omega'_Y = -\Omega_Y \left\{ \frac{\gamma}{1 + (\gamma - 1)v^2} [2\bar{Q}_0 + (1 - v^2)\bar{Q}_+ + 2v\bar{C}_1] + 2F_Y \right\}. \tag{18}$$

The reduced equations and the equation for Y are invariant under the transformation

$$(\bar{\tau}, \bar{Q}_0, \bar{Q}_+, \bar{C}_1, v) \rightarrow (-\bar{\tau}, -\bar{Q}_0, -\bar{Q}_+, \bar{C}_1, -v). \tag{19}$$

The line element can be obtained when \bar{Q}_0, \bar{C}_1 and Y have been found through the relations

$$D_1 = \sqrt{3}(Y\bar{C}_1)^{-1}, \quad D_2 = \sqrt{3}[Y^2(1 - \bar{Q}_0^2)]^{-1/2}, \quad t = \sqrt{3} \int \frac{d\bar{\tau}}{Y}. \tag{20}$$

Because of the above discrete symmetry, there are, in general, *two* orbits in the reduced phase space, related by (19), corresponding to a single line element. There is also a class of orbits that are invariant under the above discrete symmetry and in this case each orbit corresponds to a single line element.

3. Dynamical systems analysis of the reduced phase space

The reduced phase space is determined by $(\bar{Q}_0, \bar{Q}_+, \bar{C}_1, v)$, related by the constraint $G = 0$, given by equation (16). The boundary of the physical phase space is of essential importance in understanding the dynamics of the interior phase space and hence we will include it in our analysis and thus obtain a compactified phase space. We will not solve the constraint globally since this leads to problems. Instead we will follow [19, 20] and solve it locally around the equilibrium points (i.e. we will solve the linearized constraint for different variables at different equilibrium points). This formulation will enable us to achieve a good understanding of the global structure of the reduced phase space.

3.1. Equilibrium points and local analysis

Here we will present the equilibrium points together with Ω_Y , which will indicate if a point is a vacuum point or not, the gradient of the constraint and what variable we have locally solved for, and finally the eigenvalues. There are numerous equilibrium points. However, they are often closely related. We will use the following notation: the equilibrium points are denoted as

$$\text{sgn}(\bar{Q}_0) \text{Kernel}_{\text{sgn}(\bar{Q}_+)}^{\text{sgn}(v)}. \quad (21)$$

When there is no risk for confusion we will suppress $\text{sgn}(\bar{Q}_0)$, $\text{sgn}(\bar{Q}_+)$ or $\text{sgn}(v)$.

3.1.1. Equilibrium points with zero tilt, $v = 0$.

The equilibrium points $\pm F$:

$$\begin{aligned} \bar{Q}_0 &= \pm 1, \quad \bar{Q}_+ = -\frac{\bar{Q}_0}{2}, \quad \bar{C}_1 = 0; \quad \Omega_Y = \frac{3}{4}; \\ \nabla G &= (0, 0, \bar{Q}_0, \frac{3\gamma}{4}), \quad (\bar{C}_1 \text{ eliminated}); \\ \lambda_1 &= \frac{1}{2}(3\gamma - 2)\bar{Q}_0, \quad \lambda_2 = \frac{-3}{4}(2 - \gamma)\bar{Q}_0, \quad \lambda_3 = \frac{1}{4}(3\gamma - 2)\bar{Q}_0. \end{aligned} \quad (22)$$

These points are saddle points in the full phase space but there is a two-dimensional separatrix surface, spanned by the eigenvectors corresponding to the eigenvalues λ_1 and λ_3 above, the orbits of which lie in the interior of phase space.

The equilibrium points $\pm K_{\pm}^0$:

$$\begin{aligned} \bar{Q}_0 &= \pm 1, \quad \bar{Q}_+ = \bar{Q}_0, \quad \bar{C}_1 = 0; \quad \Omega_Y = 0; \\ \nabla G &= (0, 0, -2\bar{Q}_0, 0), \quad (\bar{C}_1 \text{ eliminated}); \\ \lambda_1 &= 2\bar{Q}_0, \quad \lambda_2 = 3(2 - \gamma)\bar{Q}_0, \quad \lambda_3 = (3\gamma - 2)\bar{Q}_0. \end{aligned} \quad (23)$$

The point $+K_+^0$ ($-K_-^0$) is a local source (sink). Therefore there is a two-parameter set of orbits starting (ending) at the point $+K_+^0$ ($-K_-^0$).

The equilibrium points $\pm K_{\mp}^0$:

$$\begin{aligned} \bar{Q}_0 &= \pm 1, \quad \bar{Q}_+ = -\bar{Q}_0, \quad \bar{C}_1 = 0; \quad \Omega_Y = 0; \\ \nabla G &= (0, 0, 2\bar{Q}_0, 0), \quad (\bar{C}_1 \text{ eliminated}); \\ \lambda_1 &= 2\bar{Q}_0, \quad \lambda_2 = -\lambda_3 = (2 - \gamma)\bar{Q}_0. \end{aligned} \quad (24)$$

These two points are saddle points on the boundary and there are no asymptotes into the physical phase space.

3.1.2. Equilibrium points with intermediate tilt, $0 < v^2 < 1$.

The equilibrium points $\pm \tilde{M}$:

$$\begin{aligned}
\bar{Q}_0 &= \pm 1, \quad \bar{Q}_+ = 0, \quad \bar{C}_1 = 1, \\
v &= \left[\frac{-\gamma(\gamma-1) + \sqrt{(\gamma-1)(\gamma^2(\gamma-1) + (2-\gamma)(3\gamma-2))}}{(3\gamma-2)(\gamma-1)} \right] \bar{Q}_0; \\
\Omega_Y &= 0; \\
\nabla G &= (0, -2[1 + (\gamma-1)v^2], -2\gamma v, 0), \quad (\bar{C}_1 \text{ eliminated}); \\
\lambda_1 &= -2\bar{Q}_0, \quad \lambda_2 = \frac{2\bar{Q}_0(\gamma-1)W}{(3\gamma-2)[1 - (\gamma-1)v^2]}, \\
\lambda_3 &= \frac{(1 + \bar{Q}_0 v)[(2-\gamma) + (3\gamma-2)\bar{Q}_0 v]}{-\gamma v},
\end{aligned} \tag{25}$$

where

$$W = (3\gamma-2) + 4(3\gamma-4)v\bar{Q}_0 + (3\gamma^2-4)v^2 - (3\gamma-2)(\gamma-1)v^4. \tag{26}$$

These points correspond to the Minkowski spacetime. The constraint $|v| \leq 1$ implies that these two points are physical only for $\gamma > \frac{6}{5}$. The point $+\tilde{M}$ ($-\tilde{M}$) enters the physical part of phase space though the point $+M^+$ ($-M^-$) (discussed below) at $\gamma = \frac{6}{5}$. Note the bifurcation in the eigenvalue for $\gamma = \frac{6}{5}$ in equation (28). As γ increases, $+\tilde{M}$ ($-\tilde{M}$) moves along the line $+M^+ - +M^-$ ($-M^- - -M^+$). From the expressions above, it follows that $\lambda_2 < 0$ and $\lambda_3 > 0$ for $\frac{6}{5} < \gamma < 2$. Therefore $+\tilde{M}$ ($-\tilde{M}$) is a saddle point in the full phase space. The positive (negative) eigenvalue λ_3 is associated with the vacuum submanifold so there is a two-dimensional separatrix surface ending (starting) at $+\tilde{M}$ ($-\tilde{M}$), the orbits of which lie in the interior phase space.

3.1.3. Equilibrium points with extreme tilt, $v^2 = 1$.

The equilibrium points $\pm K_{\pm}^{\pm}$:

$$\begin{aligned}
\bar{Q}_0 &= \pm 1, \quad \bar{Q}_+ = \bar{Q}_0, \quad \bar{C}_1 = 0; \quad \Omega_Y = 0; \\
\nabla G &= (0, -2\gamma \text{sgn}(v), -2\gamma \bar{Q}_0, 0), \quad (\bar{C}_1 \text{ eliminated}); \\
\lambda_1 &= 2\bar{Q}_0, \quad \lambda_2 = 4\bar{Q}_0, \quad \lambda_3 = -\frac{2(3\gamma-2)\bar{Q}_0}{2-\gamma}.
\end{aligned} \tag{27}$$

Note that the sign of v affects the linearized constraint but not the stability of the points. These points are saddle points on the boundary and there are no asymptotes into the interior phase space.

The equilibrium points $\pm M^{\pm}$:

$$\begin{aligned}
\bar{Q}_0 &= \pm 1, \quad \bar{Q}_+ = 0, \quad \bar{C}_1 = 1, \quad v = \bar{Q}_0; \quad \Omega_Y = 0; \\
\nabla G &= (0, -2\gamma, -2\gamma \bar{Q}_0, 0), \quad (\bar{C}_1 \text{ eliminated}); \\
\lambda_1 &= -2\bar{Q}_0, \quad \lambda_2 = -4\bar{Q}_0, \quad \lambda_3 = \frac{-2(5\gamma-6)\bar{Q}_0}{2-\gamma}.
\end{aligned} \tag{28}$$

These points correspond to the Minkowski spacetime. Note that there is a bifurcation at $\gamma = \frac{6}{5}$. For $1 < \gamma \leq \frac{6}{5}$ the points $\pm M^{\pm}$ are saddle points on the boundary and there

are no asymptotes entering the interior of the phase space. At $\gamma = \frac{6}{5}$ they coincide with the points $\pm \tilde{M}$ respectively. For $\frac{6}{5} < \gamma < 2$ the point ${}_+M^+$ (${}_+M^-$) is a sink (source) and there is a two-parameter set of orbits ending (starting) at the point.

The equilibrium points $\pm \mathcal{H}^\mp$:

$$\begin{aligned}\bar{Q}_0 &= \pm 1, \quad \bar{Q}_+ = -\bar{Q}_0(1 - \bar{C}_1), \quad v = -\bar{Q}_0; \\ \Omega_Y &= -2\bar{Q}_0\bar{Q}_+(1 + \bar{Q}_0\bar{Q}_+); \\ \nabla G &= (0, -2\gamma, 2\bar{Q}_0\gamma, -2(2 - \gamma)\bar{Q}_0\bar{Q}_+(1 + \bar{Q}_0\bar{Q}_+)); \\ &(\bar{C}_1 \text{ eliminated}); \\ \lambda_1 &= \lambda_2 = -2\bar{Q}_0(1 + 2\bar{Q}_0\bar{Q}_+), \quad \lambda_3 = 0.\end{aligned}\tag{29}$$

The constraint $\Omega_Y \geq 0$ implies that \bar{Q}_+ is restricted to the interval $-1 \leq \bar{Q}_+ \leq 0$ ($0 \leq \bar{Q}_+ \leq 1$) when $\bar{Q}_0 = 1$ ($\bar{Q}_0 = -1$). There is only one non-zero eigenvalue corresponding to two different eigenvectors. Equilibrium points on the line ${}_+\mathcal{H}^-$ (${}_-\mathcal{H}^+$) are sources when $-1 \leq \bar{Q}_+ < -\frac{1}{2}$ ($0 \leq \bar{Q}_+ < \frac{1}{2}$) and sinks when $-\frac{1}{2} < \bar{Q}_+ \leq 0$ ($\frac{1}{2} < \bar{Q}_+ \leq 1$).

The equilibrium points $\pm K_\mp^\mp$:

$$\begin{aligned}\bar{Q}_0 &= \pm 1, \quad \bar{Q}_+ = -\bar{Q}_0, \quad \bar{C}_1 = 0; \quad \Omega_Y = 0; \\ \nabla G &= (0, 2\gamma \text{sgn}(v), 2\gamma\bar{Q}_0, 0), \quad (\bar{C}_1 \text{ eliminated}); \\ \lambda_1 &= \lambda_2 = 2, \quad \lambda_3 = 0.\end{aligned}\tag{30}$$

These two points are the endpoints of the physical part of the lines $\pm \mathcal{H}^\mp$, respectively. They describe the boundary asymptotes which play an important role in understanding the global dynamics of phase space. This motivates their special treatment. The points $\pm K_\mp^\mp$ have no asymptotes entering the interior phase space.

The equilibrium points $\pm M^\mp$:

$$\begin{aligned}\bar{Q}_0 &= \pm 1, \quad \bar{Q}_+ = 0, \quad \bar{C}_1 = 1, \quad v = -\bar{Q}_0; \quad \Omega_Y = 0; \\ \nabla G &= (0, -2\gamma, 2\gamma\bar{Q}_0, 0), \quad (\bar{C}_1 \text{ eliminated}); \\ \lambda_1 &= \lambda_2 = -2\bar{Q}_0, \quad \lambda_3 = 0.\end{aligned}\tag{31}$$

These points correspond to the Minkowski spacetime, and are the other endpoints (compared to $\pm K_\mp^\pm$) of the lines $\pm \mathcal{H}^\mp$. These points have no asymptotes entering the interior phase space.

3.2. Invariant submanifolds on the boundary of the SSS phase space

The boundary is described by a number of invariant subsets: $\bar{Q}_0 = \pm 1$, $\Omega_Y = 1 - \bar{Q}_+^2 - \bar{C}_1^2 = 0$, $\bar{C}_1 = 0$, $v = \pm 1$. The submanifolds with $\bar{Q}_0 = \pm 1$ are described by the same equations as the reduced equations for the plane symmetric type ${}_1\text{I}$ models. The equations corresponding to the submanifolds with $v = \pm 1$ are identical to the reduced field equations for SSS spherically symmetric models with a neutrino fluid as the source. The submanifolds associated with $\Omega_Y = 0$ are vacuum submanifolds with a test fluid. The constraint (16) implies that $\bar{Q}_+\bar{C}_1 = 0$ when $\Omega_Y = 0$. If $\bar{Q}_+ = 0$, one obtains the same equations as one has for SSS spherically symmetric vacuum models

Table 1. The various boundary submanifolds.

Boundary	Restriction
$\pm 1\text{I}$	$\bar{Q}_0 = \pm 1$
V	$\Omega_Y = 0, \bar{Q}_+ = 0, \bar{C}_1 = 1$
N^\pm	$v = \pm 1$
KSV_\pm	$\Omega_Y = 0, \bar{Q}_+ = \pm 1, \bar{C}_1 = 0$
KS	$\bar{C}_1 = 0, v = 0$

with a test perfect fluid, while $\bar{C}_1 = 0$ leads to the same equations as those describing spatially homogeneous Kantowski-Sachs (KS) vacuum models with a test perfect fluid. Apart from the above vacuum submanifolds, $\bar{C}_1 = 0$ also leads to a submanifold with $v = 0$. This submanifold is described by the same equations as the orthogonal SH KS perfect-fluid models. The submanifolds are collected in Table 1 where we also introduce designations.

We will now describe the dynamical features of the individual boundary submanifolds.

The $\pm 1\text{I}$ submanifolds. The dynamical structure of the plane symmetric type $+1\text{I}$ submanifold is given in figure 1(a) ($\gamma > \frac{6}{5}$) and (b) ($\gamma \leq \frac{6}{5}$). That of -1I is easily obtained by applying the discrete symmetry (19).

The V submanifold. The dynamical structure of the V submanifold is given in figure 1(c) ($\gamma > \frac{6}{5}$) and (d) ($\gamma \leq \frac{6}{5}$). Note that \bar{Q}_0 is an increasing monotonic function.

The N^\pm submanifolds. The dynamical structure of the N^- submanifold is given in figure 1(e). That of N^+ is easily obtained by applying the discrete symmetry (19). Note that $\bar{Q}_+ \leq 0$ ($\bar{Q}_+ \geq 0$) in the N^- (N^+) case. The N^\pm submanifolds are solvable. The orbits are characterized by the following integral:

$$\frac{\bar{Q}_+ \bar{C}_1}{[\bar{Q}_0 - \bar{Q}_+ - \text{sgn}(v) \bar{C}_1]^2} = \text{constant}. \quad (32)$$

The KSV_\pm submanifolds. The dynamical structure of the KSV_- submanifold is given in figure 1(f). That of KSV_+ is easily obtained by applying the discrete symmetry (19). The variable v satisfies the inequality $v \leq 0$ ($v \geq 0$) in the KSV_- (KSV_+) submanifold. The KSV_\pm submanifolds are solvable. The integral describing the various orbits is given by

$$\frac{v}{[1 - \text{sgn}(\bar{Q}_+) \bar{Q}_0]^\gamma} \left(\frac{1 - \bar{Q}_0^2}{1 - v^2} \right)^{\frac{1}{2}(2-\gamma)} = \text{constant}. \quad (33)$$

It is worth pointing out that \bar{Q}_0 is an increasing (decreasing) monotonic function and that v is a decreasing (increasing) monotonic function for the KSV_- (KSV_+) submanifold.

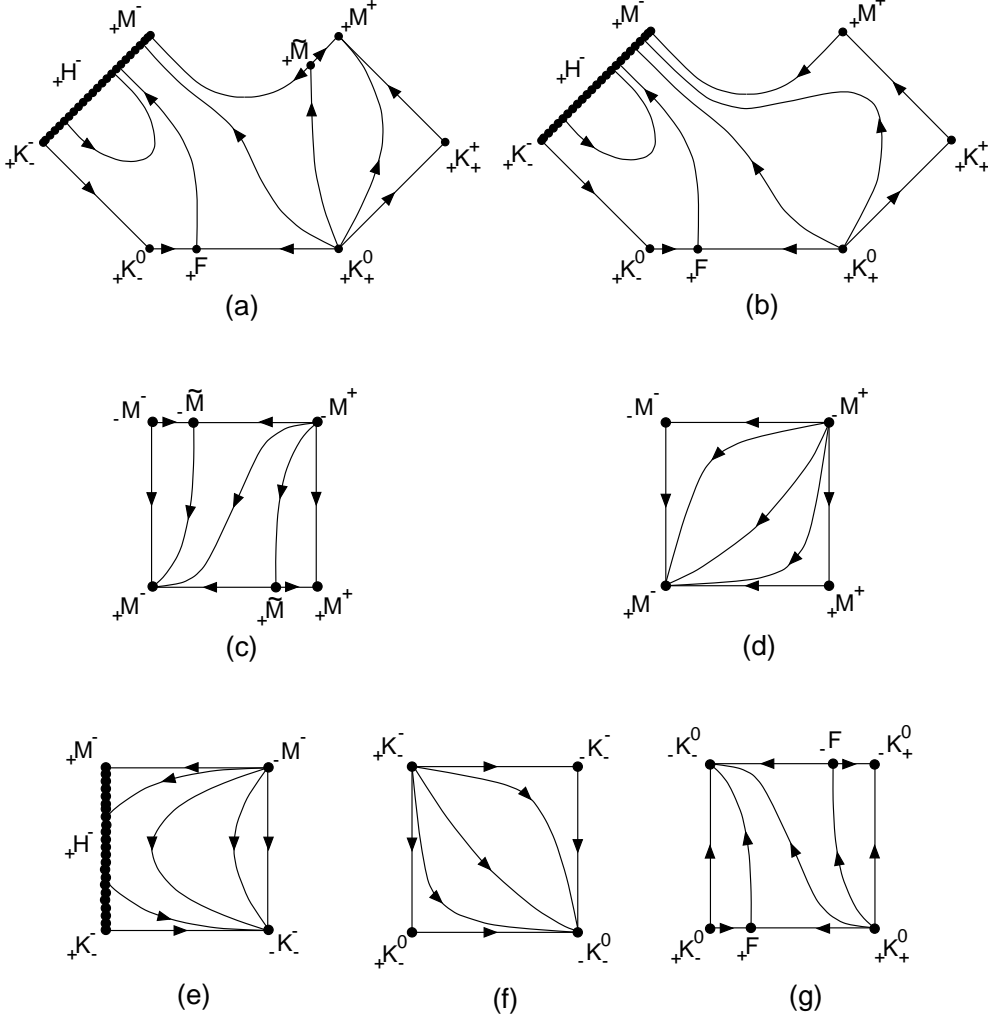


Figure 1. The phase portraits of some of the submanifolds that make up the boundary of the reduced phase space. (a) $+I$ for $\gamma > \frac{6}{5}$, (b) $+I$ for $\gamma \leq \frac{6}{5}$, (c) V for $\gamma > \frac{6}{5}$, (d) V for $\gamma \leq \frac{6}{5}$, (e) N^- , (f) KSV_- , (g) KS .

The KS submanifold. Since the equations for this submanifold are the same as those for the SH KS models we automatically, as a bonus, get a dynamical description of these models. The SH KS models are of considerable interest and have been discussed in the literature before. Collins formulated the field equations as a dynamical system and made a qualitative analysis [21]. However, he did not obtain a compact phase space. Uggla and von Zur Mühlen discussed the locally rotationally symmetric SH Bianchi type IX models [22]. The KS models appear as a boundary submanifold in this context, but this was unfortunately not pointed out in [22]. Neither was a phase portrait given. The dynamical structure of the KS submanifold is given in figure 1(g). Note that \bar{Q}_0 is a monotonic function taking the solutions from big bang to big crunch. There exists a single time-symmetric orbit invariant under the discrete symmetry (19).

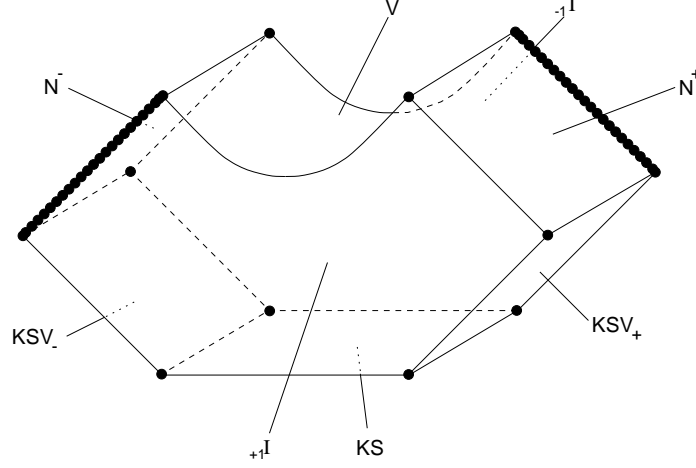


Figure 2. This picture shows how the boundary of the reduced phase space of the spatially self-similar spherically symmetric models is constructed out of the invariant submanifolds discussed in section 3.2.

There is also a single orbit starting (ending) at the point $+F$ ($-F$). The $+F$ point ($-F$ point) corresponds to the flat FLRW solution in the SH KS geometry, and consequently these models have an asymptotically flat FLRW behaviour.

Orbits in the interior phase space coming close to the KS submanifold can be approximated with KS orbits. The corresponding self-similar models in the interior phase space can thus be approximately described by a SH model multiplied by the homothetic factor, i.e. they are approximately conformally SH.

4. Global dynamical behavior

By appropriately ‘gluing together’ the boundary submanifolds of the previous section, we obtain the reduced phase space shown in figure 2, of which the SSS models are orbits in the interior. By indicating the stability of the equilibrium points on the boundary we get figure 3 for $\gamma \leq \frac{6}{5}$ and figure 4 for $\gamma > \frac{6}{5}$. The orbits on the boundary corresponding to eigenvector directions of the points $\pm F$ and $\pm \tilde{M}$ are also shown. The two-dimensional separatrix surfaces entering the interior phase space from these two points will be discussed in section 4.3.

4.1. Monotonic functions

Monotonic functions are important tools for understanding the global dynamics. For example, the existence of a monotonic function in a region of phase space implies that there cannot be any limit cycles in that region.

The function

$$M = (1 - \bar{Q}_0^2)^{2-\gamma} \bar{Q}_+^{3\gamma-4} \bar{C}_1^{-\gamma} v^2 (1 - v^2)^{-(2-\gamma)}, \quad (34)$$

whose derivative is given by

$$M' = - \left[\frac{(2-\gamma)(3\gamma-2)(1-v^2)\bar{C}_1}{\gamma v} \right] M, \quad (35)$$

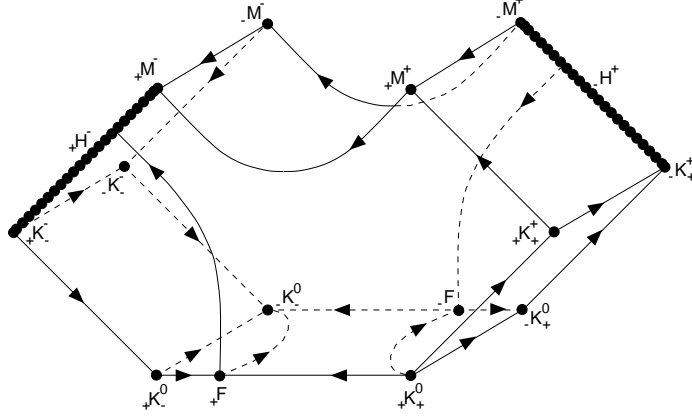


Figure 3. The reduced phase space for $\gamma \leq \frac{6}{5}$.

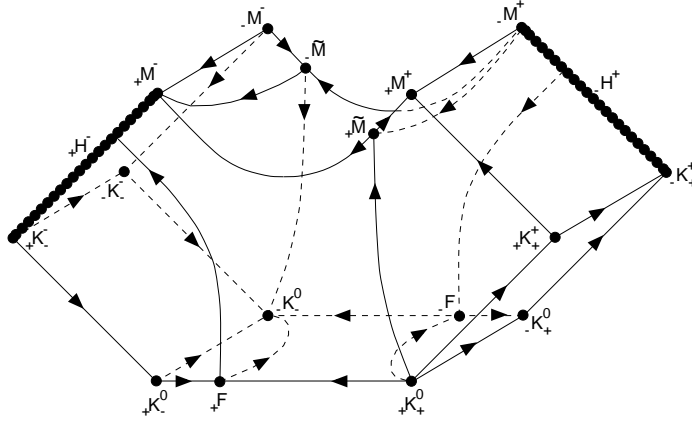


Figure 4. The reduced phase space for $\gamma > \frac{6}{5}$.

is monotone in the regions $v < 0$ and $v > 0$. There are no interior invariant submanifolds with $v = 0$. Thus all attractors (in the present case, equilibrium points) lie on the boundary.

4.2. Classification of orbits

It is natural to divide the orbits in the SSS phase space into three categories depending on the extendibility properties into the timelike self-similar (TSS) region. In order to continue an orbit into the TSS region it must start or end at an equilibrium point with extreme tilt ($|v| = 1$). The classification presented here is based on whether orbits start and/or end at $\pm \mathcal{H}^\mp$. It is also possible to extend orbits into the TSS region through $\pm M^\pm$, but from the structure of the TSS part of the phase space [17] it is clear that these orbits are not as physically interesting as the orbits starting or ending at $\pm \mathcal{H}^\mp$. The three categories are:

- 0: Orbits that are purely SSS, i.e., orbits that do not start or end at $\pm \mathcal{H}^\mp$.
- I: Orbits that may be continued into the TSS region ‘once’, e.g. orbits that start

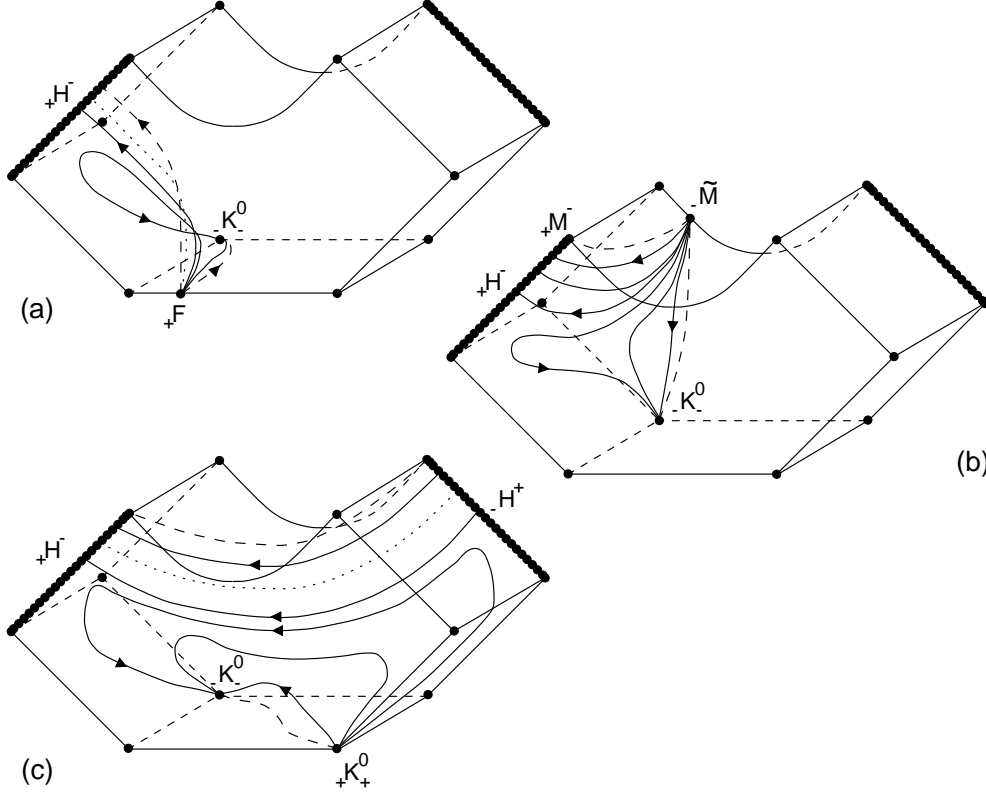


Figure 5. Separatrix submanifolds in the interior of the reduced phase space. a) The $+F$ submanifold. The dotted orbit is the FLRW-orbit. b) The $-M$ submanifold. The dotted orbit is the TOVKMZ-orbit. Dashed orbits lie in the boundary submanifolds.

(end) at an equilibrium point not belonging to $\pm\mathcal{H}^\mp$ while they end (start) at $\pm\mathcal{H}^\mp$.

II: Orbits that may be continued into the TSS region ‘twice’, e.g. orbits that start and end at $\pm\mathcal{H}^\mp$.

4.3. Invariant submanifolds in the interior of the SSS phase space

The $\pm F$ submanifolds. The separatrix surface spanned by the outgoing (ingoing) eigenvectors of the $+F$ ($-F$) point will be referred to as the $+F$ ($-F$) submanifold (figure 5(a)). The $+F$ submanifold contains two different types of orbits. Near the $+1I$ submanifold, the orbits belong to category I and end in a band on the $+\mathcal{H}^-$ line. The separatrix boundary in $+1I$ defines the upper boundary of the band. The lower boundary is for $\bar{Q}_+ = -\frac{1}{2}$, where the stability of the $+\mathcal{H}^-$ line changes to a source. The orbits in the $+F$ submanifold that are close to the Kantowski-Sachs submanifold belong to category 0. They approach $+\mathcal{H}^-$, but are repelled and end at $-K_-^0$. The structure of the $-F$ submanifold is easily obtained by applying the discrete symmetry (19). Note that for the $+F$ ($-F$) separatrix, $v < 0$ ($v > 0$) in the whole interior.

In an SH slicing, an additional homothetic Killing vector leads to solutions being represented as equilibrium points [23]. This is the case with the flat FLRW solution.

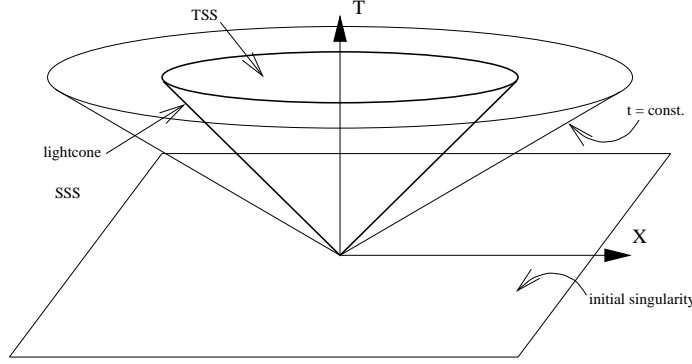


Figure 6. Schematic picture of the flat FLRW spacetime with a slicing adapted to the homothetic Killing vector, compared to a slicing adapted to the comoving time T . The cones are hypersurfaces of constant self-similar variable t . The region inside the lightcone is the TSS region. Note that the cones actually have a much more complicated structure than in this over-simplified picture.

However, in the present case we have a slicing associated with the homothetic Killing vector, see figure 6. In this formulation, the flat FLRW solution appears as an one-dimensional orbit. The SSS part of the flat FLRW solution actually corresponds to two (equivalent) orbits contained within the ‘category I band’. The FLRW orbits can be found by imposing the Petrov type 0 condition along with vanishing fluid shear and acceleration. The orbits are characterized by

$$\bar{Q}_+ = -\frac{2\bar{Q}_0}{4 + (3\gamma - 2)v^2}, \quad C_1 = -\frac{3\gamma v\bar{Q}_0}{4 + (3\gamma - 2)v^2}. \quad (36)$$

The FLRW orbit in the ${}_+F$ submanifold ends at a point on ${}_+\mathcal{H}^-$ with $\bar{Q}_+ = -2/(3\gamma + 2)$.

The invariant quantity $2m/R$ (see Appendix A.2) computed for the FLRW orbits is given by

$$\frac{2m}{R} = \frac{1}{3}\tilde{\mu}R^2 = \frac{4}{(3\gamma - 2)^2v^2}. \quad (37)$$

Note that there is a one-parameter set of orbits within the ${}_+F$ submanifold lying arbitrarily close to the FLRW orbit throughout the entire SSS region.

Self-similar fluctuations in a flat FLRW universe have been studied by Carr and Yahil [1], although they focus their discussion on phenomena pertaining to the TSS region. In order to study density perturbations, we follow Ellis and Bruni [24]. Their approach has the advantage of being covariant and gauge independent. The fractional density gradient is characterized by a quantity L (see Appendix A.3). This quantity vanishes identically for non-tilted SH models. In the present case we have two such examples, namely the flat FLRW solution and the entire KS boundary submanifold. Solutions close to the flat FLRW in the ${}_+F$ submanifold can be parametrized by L : negative values of L correspond to over-dense solutions ($\tilde{\mu} > \tilde{\mu}_{FLRW}$), and positive values correspond to under-dense solutions. Thus, the flat FLRW solution splits the ${}_+F$ submanifold into an under-dense part and an over-dense part. Over-dense solutions, starting out from the equilibrium point ${}_+F$ in a direction sufficiently close to the KS boundary, behave completely differently compared to the FLRW solution and correspond to category 0 orbits. The remaining orbits in the ${}_+F$ submanifold

behave roughly as the flat FLRW orbit and belong to category I. Near the equilibrium point ${}_+F$, the fractional density gradient vanishes to linear order. Consequently, all solutions in the ${}_+F$ submanifold are near-homogeneous initially, with density fluctuations growing significant only at later stages, possibly with the exception of the origin $r = 0$.

The $\pm\tilde{M}$ submanifolds. The equilibrium points $\pm\tilde{M}$ exist when $\gamma > \frac{6}{5}$. In this case one has additional separatrix surfaces in phase space. As for the ${}_+F$ submanifold, the orbits in the ${}_-\tilde{M}$ submanifold (figure 5(b)) are separated into two bands. Orbits starting close to the vacuum submanifold belong to category I and end on ${}_+\mathcal{H}^-$ in a continuous band from ${}_+M^-$ down to $\bar{Q}_+ = -\frac{1}{2}$. The other band contains orbits belonging to category 0, which are repelled from ${}_+\mathcal{H}^-$ and end at ${}_+K_-^0$.

The Symmetric submanifold. Orbits passing through $(\bar{Q}_0 = 0, \bar{Q}_+ = 0, \bar{C}_1, v = 0)$ constitute a submanifold containing ‘time-symmetric’ solutions (figure 5(c)). The orbits in the symmetric submanifold (S submanifold) fall into two classes: those starting at ${}_-\mathcal{H}^+$ and ending at ${}_+\mathcal{H}^-$, thus belonging to category II, and those belonging to category 0, starting at ${}_+K_+^0$ and ending at ${}_+K_-^0$.

One of the orbits in the S submanifold belonging to category II corresponds to the SSS part of a static self-similar solution associated with many names: Tolman [25], Oppenheimer and Volkoff [26], Klein [27] and Misner and Zepolsky [28], see e.g. Henriksen and Patel [13], Collins [29] and Bogoyavlensky [4]. We will call this orbit the TOVKMZ orbit. It is characterized by

$$\bar{Q}_+ = -\frac{2(\gamma-1)\bar{Q}_0}{3\gamma-2}, \quad \bar{C}_1 = -\frac{\gamma\bar{Q}_0}{(3\gamma-2)v}. \quad (38)$$

The quantity $2m/R$ takes the form

$$\frac{2m}{R} = \tilde{\mu}R^2 = \frac{4(\gamma-1)}{(2-\gamma)^2 + 8(\gamma-1)}. \quad (39)$$

4.4. General structure of interior orbits:

Here we consider the behavior of orbits, not necessarily belonging to any of the submanifolds discussed above. A general orbit must start at one of the sources of the reduced phase space, and end at one of the sinks. The analysis is performed separately for $\gamma \leq \frac{6}{5}$ and $\gamma > \frac{6}{5}$. For $\gamma \leq \frac{6}{5}$, the possible sources are the point ${}_+K_+^0$, and the ‘source parts’ of the lines ${}_+\mathcal{H}^-$ and ${}_-\mathcal{H}^+$. The only sinks are the point ${}_+K_-^0$, and the ‘sink parts’ of the lines ${}_+\mathcal{H}^-$ and ${}_-\mathcal{H}^+$. Thus there are nine possible types of orbits for $\gamma \leq \frac{6}{5}$. It seems highly unlikely that orbits starting at ${}_+\mathcal{H}^-$ and ending at ${}_-\mathcal{H}^+$ exist, especially since the ${}_+K_-^0$ sink in general is very strong. Apart from such orbits, the existence of general orbits of all categories have been verified numerically. When $\gamma > \frac{6}{5}$, the appearance of the $\pm\tilde{M}$ points changes the stability of ${}_+M^-$ to a source, and ${}_+M^+$ to a sink. Apart from all the types of orbits occurring for $\gamma \leq \frac{6}{5}$, there will be additional types of orbits. However, some of the new possible combinations of start- and end-points do not occur. This is due to the $\pm\tilde{M}$ separatrices ‘screening’ the $\pm M^\pm$ points. Thus, orbits starting at ${}_+M^-$ and ending at ${}_+M^+$ or ${}_-\mathcal{H}^+$ do not exist. Likewise, orbits starting at ${}_+\mathcal{H}^-$ and ending at ${}_+M^+$ do not appear either. Apart from these exclusions, the existence of general orbits of all categories have been verified numerically for $\gamma > \frac{6}{5}$ as well.

5. Discussion

In this paper we have used a dynamical systems approach to study the global structure of the solution space of SSS spherically symmetric perfect fluid models. By choosing variables adapted to the homothetic Killing vector field the phase space of these models can be made compact – a very desirable property. As the constraint equation for these models is not solved globally, but rather locally at the equilibrium points of the system, we avoid ‘crushing’ parts of phase space. As a result of having a complete regular phase space we find that there is a bifurcation at $\gamma = \frac{6}{5}$, something which has been overlooked in the previous literature. Also, a compact and regular phase space allows us to follow trajectories throughout their entire evolution.

It is of interest to observe that the FLRW model appears as a trajectory in phase space. This is in stark contrast to Bianchi cosmology where the flat FLRW appears as an equilibrium point. This affects the perturbation analysis of this model. In Bianchi cosmology one only needs to know the phase space in a neighbourhood of the equilibrium point. In the present case the FLRW trajectory spans most of the phase space and thus there is a need to have a full phase space description to carry out a perturbation analysis.

The existence of a monotonic function implies that there are no limit points in the interior of phase space. This stresses the importance of the boundary. The SH Kantowski-Sachs models appear as a boundary submanifold of the reduced phase space, and thus we obtain a compact description of these models as well.

We see that in the phase space corresponding to the SSS region there are models which are close to the FLRW orbit throughout their entire evolution in the SSS region. The models corresponding to these orbits can be interpreted as cosmological models with density perturbations. There are also orbits arbitrarily close to the static TOVKMZ orbit which also can be continued into the TSS region. To obtain a full spacetime picture of the models corresponding to these perturbed FLRW and static orbits, we will have to extend them into the TSS region. The TSS region will be studied in a forthcoming paper.

Appendix A. Interesting physical quantities

Appendix A.1. Fluid properties and Petrov type conditions

The fluid expansion is given by

$$\begin{aligned}\tilde{\theta} &= \frac{e^{-x}}{\sqrt{1-v^2}} \left\{ \frac{v\dot{v}}{1-v^2} + \theta + 3vB_1 \right\} \\ &= \frac{e^{-x}}{\sqrt{3}\sqrt{1-v^2}} \left\{ \frac{\sqrt{3}v\dot{v}}{1-v^2} + 2\bar{\theta} + \bar{\sigma}_+ + 3\sqrt{3}vB_1 \right\} \\ &= \frac{e^{-x}}{\sqrt{3}(1-v^2)^{3/2}} \{ vv' + (1-v^2)(2\bar{Q}_0 + \bar{Q}_+ + 3v\bar{C}_1) \} Y. \quad (\text{A.1})\end{aligned}$$

The fluid shear is given by

$$\begin{aligned}\tilde{\sigma} &= \frac{e^{-x}}{\sqrt{3}\sqrt{1-v^2}} \left\{ \frac{v\dot{v}}{1-v^2} - \sigma_+ \right\} \\ &= \frac{e^{-x}}{3(1-v^2)^{3/2}} \{ v\dot{v} - \bar{\theta} - 2\bar{\sigma}_+ \}\end{aligned}$$

$$= \frac{e^{-x}}{3(1-v^2)^{3/2}} \{vv' - (1-v^2)(\bar{Q}_0 + 2\bar{Q}_+)\} Y. \quad (\text{A.2})$$

The fluid acceleration is given by

$$\begin{aligned} \tilde{a} &= \frac{e^{-x}}{3\sqrt{1-v^2}} \left\{ \frac{3\dot{v}}{1-v^2} + \theta v - 2\sigma_+ v + 3B_1 \right\} \\ &= \frac{e^{-x}}{3\sqrt{3}(1-v^2)^{3/2}} \left\{ 3\sqrt{3}v\dot{v} - 3\bar{\sigma}_+ v + 3\sqrt{3}B_1 \right\} \\ &= \frac{e^{-x}}{\sqrt{3}(1-v^2)^{3/2}} \{v' - (1-v^2)(\bar{Q}_+ v - \bar{C}_1)\} Y. \end{aligned} \quad (\text{A.3})$$

The Weyl scalar is

$$\begin{aligned} C^2 &= C_{abcd}C^{abcd} = \frac{4}{9}e^{-4x} (3\dot{\sigma}_+ - 3B_2^2 + \theta\sigma_+ - 2\sigma_+^2)^2 \\ &= \frac{4}{9}e^{-4x} \left[\sqrt{3} \left(\dot{\bar{\theta}} + 2\dot{\bar{\sigma}}_+ \right) - 3B_2^2 - \bar{\theta}\bar{\sigma}_+ - 2\bar{\sigma}_+^2 \right]^2 \\ &= \frac{4}{9}e^{-4x} \left[\bar{Q}'_0 + 2\bar{Q}'_+ + F_Y (\bar{Q}_0 + 2\bar{Q}_+) \right. \\ &\quad \left. + \bar{Q}_0^2 - \bar{Q}_+ (\bar{Q}_0 + 2\bar{Q}_+) - 1 \right]^2 Y^4. \end{aligned} \quad (\text{A.4})$$

Note that the magnetic part of the Weyl tensor is identically zero for all models. The spacetime is of Petrov type D if $C^2 \neq 0$ and Petrov type 0 if $C^2 = 0$.

Appendix A.2. The mass function

For general spherically symmetric spacetimes the total mass-energy m between the centre distribution and some 2-space of symmetry is defined as, see e.g., Misner and Sharp [30], Hernandez and Misner [31] and Cahill and McVittie [32],

$$\frac{2m}{R} = 1 - \bar{g}^{ab} \frac{\partial R}{\partial x^a} \frac{\partial R}{\partial x^b} = \frac{1 + 2\bar{Q}_0\bar{Q}_+ + \bar{Q}_+^2 - \bar{C}_1^2}{1 - \bar{Q}_0^2}, \quad (\text{A.5})$$

where the parameter R is the invariant radius of the symmetry surfaces. By definition, the matter is outside the gravitational radius $2m$ whenever $2m/R < 1$ and inside the gravitational radius when $2m/R > 1$. The latter case is associated with the existence of an apparent horizon located at $2m/R = 1$.

Appendix A.3. Density perturbations

A covariant approach to density perturbations has been given by Ellis and Bruni [24]. The fractional density gradient is defined as

$$\Delta_a = \left(\frac{\Delta\tilde{\mu}}{\tilde{\mu}} \right)_a = \tilde{\mu}^{-1} \tilde{h}_a{}^b \tilde{\partial}_b \tilde{\mu}. \quad (\text{A.6})$$

In the reduced phase space variables, this becomes

$$\Delta_a = Y e^{-x} \frac{L}{1-v^2} (-v, 1, 0, 0), \quad (\text{A.7})$$

where

$$L = -\frac{2\bar{C}_1 [1 + (\gamma - 1)v^2] + \gamma v [2\bar{Q}_0 + (1 + v^2)\bar{Q}_+]}{\sqrt{3} [1 - (\gamma - 1)v^2]}, \quad (\text{A.8})$$

and Y is the decoupled variable (10).

Appendix B. Coordinate and variable transformations

Here we will give transformations to other coordinates and variables which have been used in the literature to study self-similar spherically symmetric models. The present variables lead to a compact and regular description everywhere in the SSS region. This is not the case with previously used variables, as is easily seen in the equations below. The simple algebraic relations make it easy to identify the points, or even manifolds, where the breakdowns occur.

Appendix B.1. The comoving (fluid) approach

The most commonly used approach is the fluid approach, where one uses a coordinate system adapted to the fluid velocity. The line element, of the presently considered SSS spherically symmetric models, takes the following form in the fluid approach (see, e.g., [7]):

$$ds^2 = -e^{\Psi(\lambda)} dT^2 + e^{\Lambda(\lambda)} dX^2 + Y^2(\lambda) X^2 d\Omega^2, \quad (\text{B.1})$$

where $\lambda = X/T$ and $d\Omega^2 = d\theta^2 + \sin^2(\theta) d\varphi^2$. The fluid velocity, u^a , is given by $e^{-\Psi/2}(1, 0, 0, 0)$.

The following transformation:

$$X = e^{x-F(\bar{t})}, \quad T = e^{x-F(\bar{t})+\bar{t}}, \quad (\text{B.2})$$

where

$$\frac{dF}{d\bar{t}} = -\frac{e^{\Psi+2\bar{t}}}{e^\Lambda - e^{\Psi+2\bar{t}}}, \quad (\text{B.3})$$

leads to the ‘homothetic’ adapted SSS spherically symmetric line element

$$ds^2 = e^{2x} d\bar{s}^2 = e^{2x} [-N^2 d\bar{t}^2 + D_1^2 dx^2 + D_2^2 d\Omega^2], \quad (\text{B.4})$$

where

$$\begin{aligned} N^2 &= e^{\Lambda+\Psi+2\bar{t}-2F} (e^\Lambda - e^{\Psi+2\bar{t}})^{-1}, \\ D_1^2 &= e^{-2F} (e^\Lambda - e^{\Psi+2\bar{t}}), \quad D_2^2 = e^{-2F} Y^2. \end{aligned} \quad (\text{B.5})$$

The fluid velocity v is given by $v^2 = e^{\Psi+2\bar{t}-\Lambda}$. Inserting this into the above expressions we find that

$$\frac{dF}{d\bar{t}} = -\frac{v^2}{1-v^2}, \quad N^2 = \frac{v^2 e^{\Lambda-2F}}{1-v^2}, \quad D_1^2 = (1-v^2) e^{\Lambda-2F}. \quad (\text{B.6})$$

The fluid approach was used by Foglizzo and Henriksen [33], see also Bicknell and Henriksen [6], to write the self-similar spherically symmetric equations in a very simple way. Their variables are related to those used in this paper according to

$$N_{F-H} = \frac{3\gamma^2 v^2 \mu_n}{4[1 + (\gamma - 1)v^2] B_1^2} = \frac{3\gamma v \bar{\sigma}_+}{2\sqrt{3} B_1} = \frac{3\gamma v \bar{Q}_+}{2\bar{C}_1} \quad (\text{B.7})$$

$$\begin{aligned} \mu_{F-H} &= \frac{[1 + (\gamma - 1)v^2] [(\bar{\theta} + \bar{\sigma}_+)^2 + 3B_2^2 - 3B_1^2]}{(1-v^2) \mu_n} \\ &= \frac{\sqrt{3}\gamma v [(\bar{\theta} + \bar{\sigma}_+)^2 + 3B_2^2 - 3B_1^2]}{2B_1 \bar{\sigma}_+ (1-v^2)} \\ &= \frac{3\gamma v (1 + 2\bar{Q}_0 \bar{Q}_+ + \bar{Q}_+^2 - \bar{C}_1^2)}{2\bar{C}_1 \bar{Q}_+ (1-v^2)} \end{aligned} \quad (\text{B.8})$$

$$v_{F-H} = v^{-1}. \quad (\text{B.9})$$

Appendix B.2. The Schwarzschild approach

The usual way to represent a spherically symmetric line element is of the form

$$ds^2 = -FdT^2 + GdR^2 + R^2d\Omega^2 \quad (\text{B.10})$$

where, in the self-similar case, F and G are functions of R/T only. The following transformation:

$$R = e^x B_2^{-1}, \quad T = e^{x+\phi(t)}, \quad (\text{B.11})$$

where the function ϕ satisfies

$$\frac{d\phi}{dt} = \frac{\sqrt{3}B_1^2}{\bar{\theta} + \bar{\sigma}_+} = \frac{\bar{C}_1^2 Y}{\sqrt{3}(\bar{Q}_0 + \bar{Q}_+)}, \quad (\text{B.12})$$

transforms the line element equation (B.10) into the homothetic form. The metric functions F and G can be written as

$$F = \frac{(\bar{\theta} + \bar{\sigma}_+)^2 e^{-2\phi}}{B_1^2 [3B_1^2 - (\bar{\theta} + \bar{\sigma}_+)^2]} = \frac{3(\bar{Q}_0 + \bar{Q}_+)^2 e^{-2\phi} Y^{-2}}{\bar{C}_1^2 [\bar{C}_1^2 - (\bar{Q}_0 + \bar{Q}_+)^2]}, \quad (\text{B.13})$$

$$G = \frac{3B_2^2}{3B_1^2 - (\bar{\theta} + \bar{\sigma}_+)^2} = \frac{1 - \bar{Q}_0^2}{\bar{C}_1^2 - (\bar{Q}_0 + \bar{Q}_+)^2}. \quad (\text{B.14})$$

Identifying $2m/R = 1 - G^{-1}$ leads to equation (A.5).

The radial 3-velocity v_R of the fluid is given by

$$v_R = \frac{\sqrt{3}vB_1 + \bar{\theta} + \bar{\sigma}_+}{\sqrt{3}B_1 + v(\bar{\theta} + \bar{\sigma}_+)} = \frac{v\bar{C}_1 + \bar{Q}_0 + \bar{Q}_+}{\bar{C}_1 + v(\bar{Q}_0 + \bar{Q}_+)}. \quad (\text{B.15})$$

In their treatment of self-similar spherically symmetric collapse, Ori and Piran [7] used the following set of variables:

$$\mathcal{M} = \frac{m}{R} = \frac{(\bar{\theta} + \bar{\sigma}_+)^2 + 3B_2^2 - 3B_1^2}{6B_2^2} = \frac{1 + 2\bar{Q}_0\bar{Q}_+ + \bar{Q}_+^2 - \bar{C}_1^2}{2(1 - \bar{Q}_0^2)} \quad (\text{B.16})$$

$$D = \frac{(1 - v^2)\mu_n}{2(1 + (\gamma - 1)v^2)B_2^2} = \frac{\sqrt{3}B_1\bar{\sigma}_+(1 - v^2)}{6\gamma vB_2^2} = \frac{\bar{C}_1\bar{Q}_+(1 - v^2)}{2\gamma v(1 - \bar{Q}_0^2)} \quad (\text{B.17})$$

$$u^r = \frac{\sqrt{3}vB_1 + \bar{\theta} + \bar{\sigma}_+}{\sqrt{3}B_2\sqrt{1 - v^2}} = \frac{v\bar{C}_1 + \bar{Q}_0 + \bar{Q}_+}{\sqrt{(1 - \bar{Q}_0^2)(1 - v^2)}}. \quad (\text{B.18})$$

The variables of Maison [9] are just

$$A_M^2 = \frac{3B_1^2 - (\bar{\theta} + \bar{\sigma}_+)^2}{3B_2^2} = \frac{\bar{C}_1^2 - (\bar{Q}_0 + \bar{Q}_+)^2}{1 - \bar{Q}_0^2}, \quad (\text{B.19})$$

$$B_M^2 = \frac{3B_1^2}{(\bar{\theta} + \bar{\sigma}_+)^2} = \frac{\bar{C}_1^2}{(\bar{Q}_0 + \bar{Q}_+)^2}, \quad (\text{B.20})$$

$$\begin{aligned} \tilde{\rho}_M &= 4\pi R^2 \tilde{\mu} = \frac{(1 - v^2)\mu_n}{2B_2^2 [1 + (\gamma - 1)v^2]} \\ &= \frac{(1 - v^2)\Omega_Y}{2(1 - \bar{Q}_0^2) [1 + (\gamma - 1)v^2]}, \end{aligned} \quad (\text{B.21})$$

$$v_M = v_R. \quad (\text{B.22})$$

References

- [1] Carr B J and Yahil A 1990 *Astrophys. J.* **360** 330
- [2] Carr B J and Coley A A Self-similarity in general relativity *Preprint*
- [3] Cahill M E and Taub A H 1971 *Commun. Math. Phys.* **21** 1
- [4] Bogoyavlensky O I 1985 *Methods in the Qualitative Theory of Dynamical Systems in Astrophysics and Gas Dynamics* (Berlin: Springer)
- [5] Carr B J and Hawking S W 1974 *Mon. Not. R. Astron. Soc.* **168** 399
- [6] Bicknell G V and Henriksen R N 1978 *Astrophys. J.* **225** 237
- [7] Ori A and Piran T 1990 *Phys. Rev. D* **42** 1068
- [8] Koike T, Hara T and Adachi S 1995 *Phys. Rev. Lett.* **74** 5170
- [9] Maison D 1996 *Phys. Lett.* **366B** 82
- [10] Coley A A 1997 *Class. Quantum Grav.* **14** 87
- [11] Moschetti G 1987 *Gen. Rel. Grav.* **19** 155
- [12] Anile A M, Moschetti G and Bogoyavlenski O I 1987 *J. Math. Phys.* **28** 2942
- [13] Henriksen R N and Patel K 1991 *Gen. Rel. Grav.* **23** 527
- [14] Eardley D M 1974 *Commun. Math. Phys.* **37** 287
- [15] Wu C 1981 *Gen. Rel. Grav.* **13** 625
- [16] Nilsson U S and Uggla C 1997 *Class. Quantum Grav.* **14** 1965
- [17] Goliath M, Nilsson U S and Uggla C 1997 in preparation
- [18] Kramer D, Stephani H, MacCallum M and Herlt E 1980 *Exact Solutions of Einstein's Field Equations* (Cambridge: Cambridge University Press)
- [19] Nilsson U and Uggla C 1996 *Class. Quantum Grav.* **13** 1601
- [20] Hewitt C G and Wainwright J 1992 *Phys. Rev. D* **46** 4242
- [21] Collins C B 1977 *J. Math. Phys.* **18** 2116
- [22] Uggla C and von Zur Mühlen H 1990 *Class. Quantum Grav.* **7** 1365
- [23] Jantzen R T and Rosquist K 1986 *Class. Quantum Grav.* **3** 281
- [24] Ellis G F R and Bruni M 1989 *Phys. Rev. D* **40** 1804
- [25] Tolman R C 1939 *Phys. Rev.* **55** 364
- [26] Oppenheimer J R and Volkoff G M 1939 *Phys. Rev.* **55** 374
- [27] Klein O 1947 *Ark. Mat. Astr. Fys.* **34A** N:o 19 1
- [28] Misner C W and Zolpolsky H S 1964 *Phys. Rev. Lett.* **12** 635
- [29] Collins C B 1985 *J. Math. Phys.* **26** 2268
- [30] Misner C W and Sharp D H 1964 *Phys. Rev. B* **136** 571
- [31] Hernandez W C and C W Misner 1966 *Astrophys. J.* **143** 452
- [32] Cahill M E and G C McVittie 1970 *J. Math. Phys.* **11** 1382
- [33] Foglizzo T and Henriksen R N 1993 *Phys. Rev. D* **48** 4645